ACS Catalysis

Research Article

pubs.acs.org/acscatalysis

Integrated Networks of Mesoporous Silica Nanowires and Their Bifunctional Catalysis−Sorption Application for Oxidative Desulfurization

Jian Dou[†] and Hua Chun Zeng*[,†,‡]

[†]Department of Chemical and Biomolecular Engineering, Faculty of Engineering, National University of Singapore, 10 Kent Ridge Crescent, Singapore 119260

[‡]Institute of Materials Research and Engineering (IMRE), 3 Research Link, Singapore 117602

Supporting Information

ABSTRACT: Integration of nanostructured mesoporous silica and related functional materials into larger assemblages will benefit their applications across various technological fields including heterogeneous catalysis, separation, sensing, drug delivery, and other applications because such assembled nanosilica can be handled in a way similar to conventional materials after use. In this work, we develop a synthetic route to synthesize and integrate thin mesoporous silica nanowires into three-dimensional (3D) networks. Hierarchical pore structures can be attained, respectively, from texture and framework mesopores within the networks. To explore their applicability, the networked nanowires have been used to support molybdenum oxide and tested for oxidative desulfurization (ODS) of model diesels. Because of the highly accessible porosity in this silica architecture, excellent activity for conversion of dibenzothiophene ($C_{12}H_8S$) to dibenzothiophene sulfone ($C_{12}H_8O_2S$) has been achieved. Quite surprisingly, the nanowire-based molybdenum catalysts can also serve as effective adsorbents for removal of product compound $C_{12}H_8O_2S$. In this regard, the materials system can function integrally both as a catalyst and as an adsorbent for the ODS process. Investigation on the formation of 3D silica nanowires has been conducted by varying synthetic parameters, and robust recyclability of the catalyst−adsorbent system has also been demonstrated.

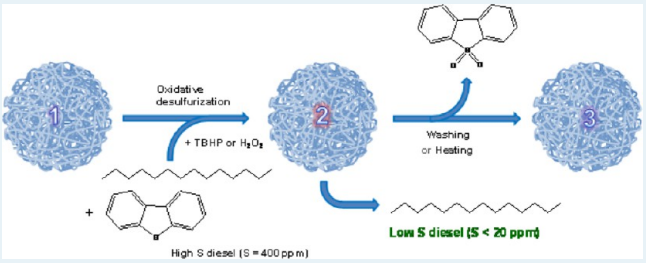

KEYWORDS: *mesoporous silica, nanowires, hierarchical, molybdenum oxide, catalyst−sorbent, oxidative desulfurization*

INTRODUCTION

Mesoporous silica and its related composites are a class of fascinating functional materials, and they have attracted enormous research interest over the past two decades.[1−28] With respect to their practical applications such as in catalysis, separation, adsorption, and drug delivery, however, it is important to take further control over their porosity, size, shape, morphology, composition, chemical/thermal stability, and process reusability.[1,2] In this regard, advanced syntheses of mesoporous silica into spheres,[3−5] fibers and rods,[6−14] wires and tubes,[15−18] monoliths,[19] and hollowed structures[20−23] have been conducted.

There have been many preparative strategies to make mesoporous silica into one-dimensional (1D) micro- and nanostructures which can be used as waveguides and laser materials.[11,24] For example, such 1D silica materials have been prepared by spinning method with a mean diameter of 40 μm.[6] Anodic aluminum membrane has also been utilized as a template to synthesize mesoporous silica fibers with an average diameter of ≈250 nm.[7] Furthermore, mesoporous silica fibers with diameters of 1 to 15 μm, whose mesopore channels (hexagonally packed) are parallel to the axial direction of the fibers, have also been prepared by a two-phase solution method.[11] It was proposed that silica films first formed at the interface of water and oil phases, followed by nucleating and growing silica fibers on the water phase side of the film. Therefore, it is important to kinetically control the hydrolysis rate of the silicate species at the water and oil interface. Later, it was found that silica fibers with diameters of 50−300 nm could be grown in (one-phase) aqueous solution as well under acidic condition, and a circular or a longitudinal pore architecture could be further selected.[10] Other synthetic parameters such as silica precursor, cosolvent, cosurfactant, static condition, and weak acid were also identified to be essential to control the morphology of fibers/nanowires.[8,12−14,17] It has been recognized that the pore architecture within the silica materials is of paramount importance for practical applications.[25,26] Furthermore, engineering mesoporous silica with multimodal pore systems (i.e., with hierarchical pore profiles) provides additional advantages for mass transport taking place in both reaction and sorption processes.[3,27,28] In addition to nominal surface area and porosity, orientation or architecture of the mesopores is

Received: October 30, 2013
Revised: January 3, 2014
Published: January 8, 2014

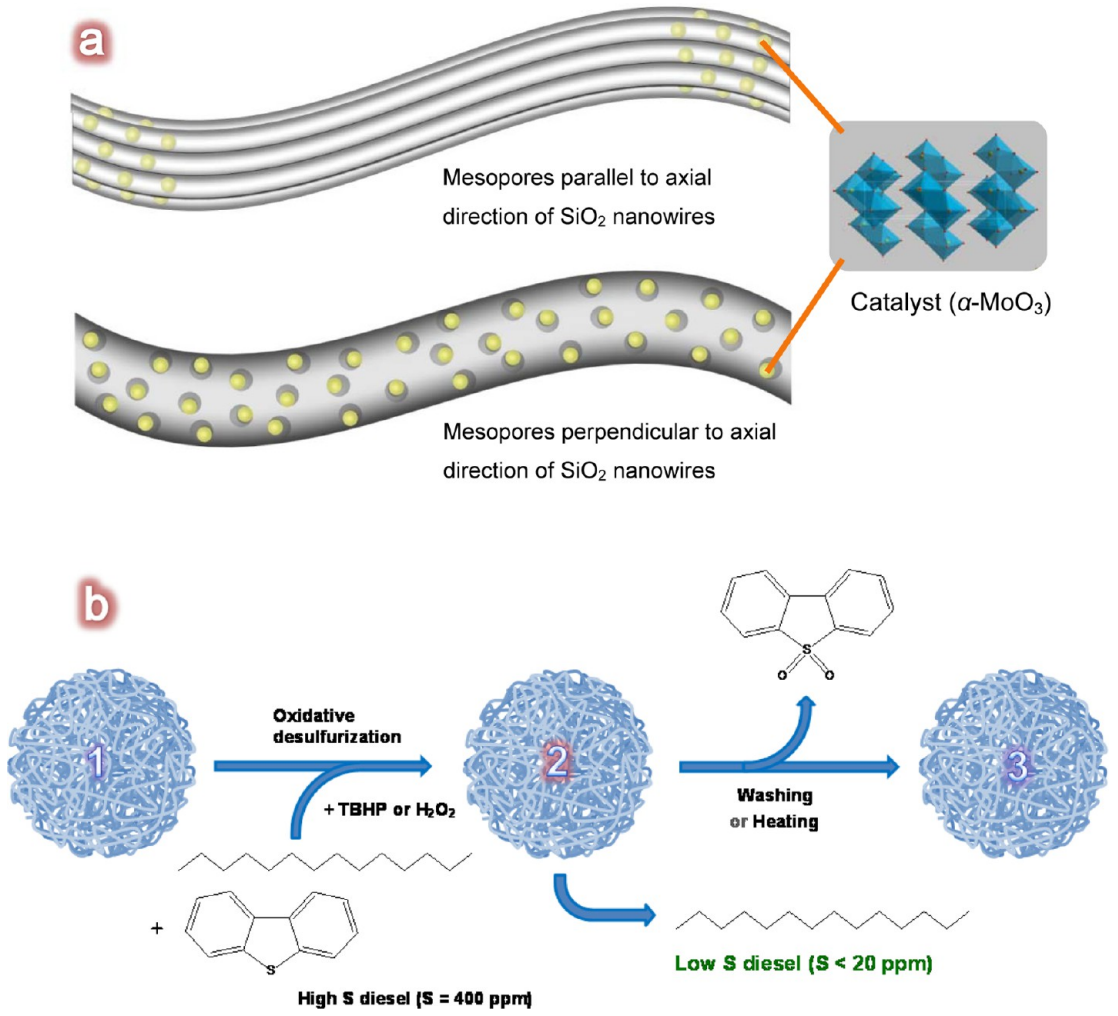

Figure 1. (a) Illustrations of catalyst nanoparticles loaded on two different types of silica nanowires (mesopores parallel to axial direction of SiO_2 nanowires and mesopores perpendicular to axial direction of SiO_2 nanowires), and (b) dual functions (catalyst + adsorbent) of Mo/*m*SiO_2 (*m* denotes mesoporous) in the present investigation of oxidative desulfurization process (**1**: fresh Mo/*m*SiO_2 nanowires, **2**: dibenzothiophene sulfone adsorbed Mo/*m*SiO_2 nanowires, and **3**: washed Mo/*m*SiO_2 nanowires (i.e., equivalent to **1**); intricate thin threads represent networked Mo/*m*SiO_2 nanowires with mesopores perpendicular to the axial direction (which is detailed in (a)).

another important structural property. For instance, regarding their catalytic applications, pore channels around, parallel, or perpendicular to the axis of the 1D silica fibers/nanowires will determine ultimate performance of working catalysts. As illustrated in Figure 1a, mesopores parallel to the axial direction of silica nanowires may lead to limited catalyst loading and a less-accessible working surface area because of the blockage of impregnated catalysts in the openings of longitudinal channels. On the other hand, shorter mesopores perpendicular to the axial direction of silica nanowires would allow more controllable catalyst impregnation and larger effective surface areas for catalytic reactions and/or sorption processes.

In consideration for applications of the above silica materials, in this work, we use deep desulfurization reaction as a testing example to illustrate their workability. Deep desulfurization of diesel fuel has received great research attention due to more stringent environmental regulations imposed over the last two decades (Table S1).[29] In the oil refinery industry, the hydrodesulfurization (HDS) process has been used for several decades to reduce the sulfur content to a level of ~500 ppm. To further reduce the sulfur to a level below 50 ppm (i.e., deep desulfurization), the HDS process has to be operated under even severer conditions (high temperature and high pressure), which are energy intensive and require hydrogen consumption. In searching for other alternatives, oxidative desulfurization (ODS) has been considered to be a complementary route to the HDS process for deep desulfurization, due to its moderate operating conditions and facile integration to existing refinery plants.[30] In eq 1, the least-reactive organosulfur compounds,

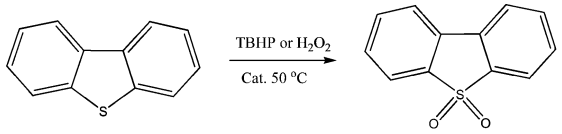

dibenzothiophene dibenzothiphene sulfone (1)

such as dibenzothiophene ($C_{12}H_8S$) and other alkyl substituted derivatives, can be more easily oxidized in the ODS reaction and subsequently removed through adsorption or extraction. There have been a number of solid-state ODS catalysts reported in literature which include heteropolyacids,[31−33] metal oxides (i.e., MnO_2, MoO_3, and WO_3),[34−41] and Ti-molecular sieves coupled with oxidants such as peroxides and air.[42−44]

dx.doi.org/10.1021/cs400996j | *ACS Catal.* 2014, 4, 566−576

Nevertheless, we note that the reported ODS processes require multiple steps for removal of reaction products, and there have not been any "one-pot" operations (i.e., reaction-cum-separation) so far. In this regard, if both reaction and separation can be integrated into a single step, the proposed ODS processes would become even more attractive, but the ODS catalysts would then be required to function as sorbents for separation as well.

As mentioned earlier, the preparation of mesoporous silica nanowires with a diameter less than 50 nm remains to be explored.[16,17] Furthermore, the architecture of pore channels is an important issue for their catalytic and sorptive applications. Aiming at these two major challenging objectives, herein, we have developed a simple chemical route to prepare interlinked mesoporous silica (mSiO$_2$) nanowires. The synthesis parameters such as cosolvent, surfactant, alkaline, reaction time, and aging temperature have been investigated thoroughly in this work to gain an understanding on the formation mechanism. The networked mSiO$_2$ nanowires have been used as a catalyst support for molybdenum (Mo/mSiO$_2$, Mo in the form of α-MoO$_3$), and the integrated Mo/mSiO$_2$ catalyst−adsorbent system has been tested for ODS application with model diesels, as illustrated in Figure 1b. It is also noteworthy to mention that while the diameters of silica nanowires have been reduced significantly to a spatial region of only 10 to 20 nm in this work, we are actually able to integrate them and increase the final dimensions of integrated networks to micrometer scale, which allows easy separation of the materials after use.[21]

EXPERIMENTAL SECTION

Preparation of Mesoporous Silica (mSiO$_2$) Nanowire Networks. Three-dimensionally interlinked mesoporous silica nanowires were synthesized by hydrolysis of tetraethyl orthosilicate (TEOS, Fluka) with triethanolamine (TEA, Acros Organics) as an alkaline source (see Table S2). In a typical synthesis, 13 mL of deionized water was first mixed with 1.0 mL of ethanol, followed by addition of 2.0 mL of 25% hexadecyltrimethylammonium chloride (CTACl, Sigma-Aldrich) aqueous solution and 0.9 mL of triethanolamine (TEA, Acros). The resultant mixture was stirred at room temperature for 30 min. Afterward, 0.5−1.5 mL of TEOS was added to the above mixture under magnetic stirring. Finally, the mixture was heated in an electric oven at 60 °C for 2 h. The resultant opaque networked mSiO$_2$ nanowires were precipitated by adding ethanol and centrifuged at 5000 rpm for 3 min.

Preparation of Mo/mSiO$_2$ Network Catalysts. The above mesoporous silica networked nanowires were heated at 550 °C in air for 6 h with a heating rate of 1°/min. The heated sample was ground into powder and used as catalyst support for molybdenum oxide with metal Mo loading of 2−15% (wt %) via impregnation with hexammonium heptamolybdate 4-hydrate (AHM, $(NH_4)_6Mo_7O_{24}\cdot 4H_2O$, Merck). The impregnated sample was calcined at 500 °C in air again for 3 h. Commercial fumed silica (Sigma-Aldrich) and aluminum oxide (Alfa Aesar) were also impregnated with 10% Mo as reference catalysts (named as Mo/SiO$_2$ and Mo/Al$_2$O$_3$, respectively).

Oxidative Desulfurization (ODS) of Model Diesel. Model diesel with sulfur (S) content of 400 ppm was prepared by dissolving 460 mg of dibenzothiophene (DBT, $C_{12}H_8S$, Alfa Aesar) in 200 mL of n-tetradecane (Alfa Aesar); 1 ppm is defined as 1 mg of sulfur atoms per liter of n-tetradecane. Liquid phase oxidative desulfurization of model diesel was carried out in a 25 mL two-necked round-bottom flask coupled in a temperature-controlled oil bath. In a typical run, 10 mL of model diesel was mixed with 0.1 mL of undecane ($C_{11}H_{24}$, as an internal standard for gas chromatography (GC)), followed by addition of 50 mg of catalyst (i.e., Mo/mSiO$_2$, or Mo/SiO$_2$ and Mo/Al$_2$O$_3$) and 57 μL of $tert$-butyl hydroperoxide solution (TBHP, $C_4H_{10}O_2$, 5.5 M in decane ($C_{10}H_{22}$), Sigma-Aldrich). The oxidant to sulfur mole ratio (TBHP/DBT) was fixed at 2.5. The reaction proceeded under vigorous stirring at 50 °C. The concentration of DBT was monitored using gas chromatography (GC, Agilent-7890A) equipped with a flame ion detector (FID) and a HP-5 column (30 m × 0.32 mm × 0.25 μm). Gas chromatography−mass spectrometry (GC-MS, Agilent, 7890A-5975C) was also used to identify chemicals before and after the ODS reaction.

Regeneration of Mo/mSiO$_2$ Catalyst−Adsorbent. The used catalysts were recycled from the reaction mixture and regenerated by either washing with 4.0 mL of toluene (repeated 5 times, as no dibenzothiophene sulfone ($C_{12}H_8O_2S$) peak was detected by GC after washing) or simply calcined in air at 400 to 500 °C for 3 h to burn off adsorbed dibenzothiophene sulfone from the oxidation reaction.

Material Characterization. The crystallographic structure of the solid samples was investigated using powder X-ray diffraction (XRD, Bruker D8 Advance, Cu Kα radiation, λ = 1.5406 Å) at a scanning rate of 1°/min. The dimension, morphology, and chemical composition of the solid samples were examined using field-emission scanning electron microscopy and energy-dispersive X-ray spectroscopy (FESEM/EDX, JSM-5600LV), transmission electron microscopy (TEM, JEM2010, 200 kV), and high-resolution transmission electron microscopy (HRTEM/EDX, JEM2100F, 200 kV). Surface and texture properties of the samples were studied by nitrogen adsorption−desorption isotherms (Quantachrome NOVA-3000 system) at 77 K. Prior to measurements, the samples were degassed at 200 °C overnight. Specific surface areas of the samples were determined using the Brunauer−Emmett−Teller (BET) method. The total pore volume was measured at relative pressure from 0.928 to 0.936 of desorption curve, and the pore size distribution was estimated using nonlocal density function theory (NLDFT) from adsorption curve.[45] Surface composition of the samples were analyzed with X-ray photoelectron spectroscopy (XPS, AXIS-HSi, Kratos Analytical) using a monochromatized Al Kα exciting radiation ($h\nu$ = 1486.71 eV). The XPS spectra of all studied elements were measured with a constant analyzer-pass-energy of 40.0 eV, and all binding energies (BE) were referenced to the Si 2p peak (BE = 103.3 eV) from the mesoporous silica support. Chemical bonding information of the samples was acquired with Fourier transform infrared spectroscopy (FTIR, Bio-Rad FTS-135) using the potassium bromide (KBr) pellet technique. To make the KBr pellets, about 1 mg of sample was diluted with 100 mg of KBr powders. Each FTIR spectrum was collected after 16 scans with a resolution of 4 cm^{-1} from 400 to 4000 cm^{-1}. Thermal behavior of the used catalyst was also investigated with thermogravimetric analysis (TGA, Shimazu, DTG-60 AH) under an air stream (100 mL/min).

RESULTS AND DISCUSSION

Synthesis and Pore Structures of mSiO$_2$ Open Networks. Under the alkaline condition, interlinked mesoporous silica nanowires (mSiO$_2$) with uniform diameters were synthesized successfully using TEOS as a silicon precursor and CTACl as a surfactant in water/ethanol mixed solvents. The TEM image of Figure 2a (and Supporting Information, Figure S1) represents a panoramic view of as-prepared mesoporous silica nanowires, which are interconnected into 3D networks. The diameters of these mesoporous silica nanowires are only around 14 nm, as can be seen in the TEM images of Figure 2b−d at higher magnifications. Interestingly, the aspect ratio of the networked mSiO$_2$ nanowires (i.e., straight portions of ligaments in the mSiO$_2$ network) could be finely tuned from ∼2:1 to 5:1 by adjusting the amount of TEOS used in the synthesis from 1.5 to 0.5 mL (Experimental Section). When the reaction mixture is stirred (instead of the standard static condition; Experimental Section), the aspect ratio could be further reduced to ∼1:1 (the synthesis was carried out in an oil bath at 60 °C; Figure S2). It is thus understood that more branches from mesoporous silica nanowires can be attained with a higher concentration of precursor molecules under more

dx.doi.org/10.1021/cs400996j | ACS Catal. 2014, 4, 566−576

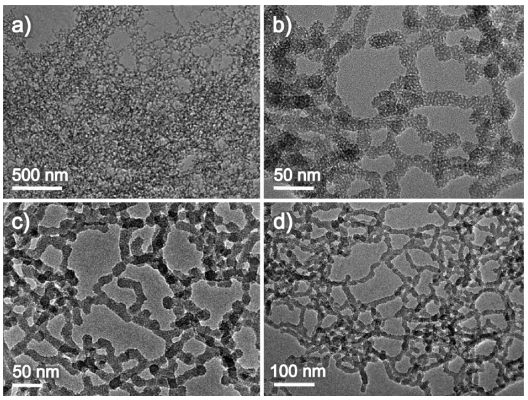

Figure 2. TEM images of interlinked mesoporous silica nanowires: (a) a large-scale view (1.0 mL of TEOS). (b–d) Aspect ratio of silica nanowires was adjusted from ~2:1 to ~5:1 by reducing the amount of TEOS used in the synthesis solution from 1.5 mL (b) to 1.0 mL (c), and to 0.5 mL (d).

buoyant convections. The branching will reduce the length of nanowires, leading to smaller aspect ratios for the ligaments in the 3D networks. Importantly, the diameter of mesoporous silica nanowires remains quite similar at ~14 nm despite varying synthetic parameters. The mesopores are randomly distributed within the silica nanowires, but they are aligned perpendicularly to the axis of nanowires (Figure S3); they are different from orderly arranged mesopore channels (either the circular or longitudinal pore architecture[10]). Quite encouragingly, the small diameters in the nanowires and open short channel pores are highly desirable because they possess more active sites and permit rapid mass transport for catalytic and sportive applications, as depicted in Figure 1a.

The above networked mSiO$_2$ nanowires were characterized by N_2 adsorption–desorption analysis at 77 K. Shown in Figure 3a, the N_2 adsorption–desorption isotherm for the mSiO$_2$ sample synthesized with 0.5 mL of TEOS can be classified as type IV with a type H1 hysteresis loop. The initial uptake of N_2 at below relative pressure of 0.1 is due to monolayer adsorption of N_2 on the walls of mesopores. At relative pressure of 0.2–0.4, the adsorption step is associated with capillary condensation in the mesopores. The last adsorption step above relative pressure of 0.8 is assigned to condensation in void spaces among the silica nanowires. The pore size distribution calculated by the NLDFT method further confirms the hierarchical pore structures (Figure 3b). A sharp peak centered at 3.6 nm indicates the presence of very uniform mesopores within the silica nanowires. The broad peak around 19.9 nm is due to void spaces among neighboring mesoporous silica nanowires (i.e., network textural pores). The presence of larger such textural mesoporosity would be beneficial as it increases the diffusibility of chemicals when accessing to the smaller mesopores. With 1.0 or 1.5 mL of TEOS used in the synthesis, the size of the primary mesopores remains basically unchanged at 3.4–3.5 nm, while the mean secondary mesopore increases to 25.4 and 32.5 nm, respectively (Figure 3c–f). A small-angle X-ray scattering study was further carried out to determine the mesopore structures, as displayed in Figure 3g. Only a weak broad peak at around 2θ = 2.1 to 2.2° (d_{100} = 4.2 to 4.0 nm) is observed for silica nanowires synthesized with 1.0 and 1.5 mL of TEOS, which is associated with wormhole-type mesopores.[4] No diffraction peaks are observable in the range of 1–10° for the mSiO$_2$ sample prepared with 0.5 mL of TEOS, indicating the presence of randomly arranged mesopores.

Formation Mechanism of mSiO$_2$ Networks. To understand the formation mechanism of interlinked mesoporous silica nanowires, the synthesis process was monitored by withdrawing a small portion of the reaction mixture during thermal treatment at 60 °C and examined with TEM technique. After being heated in an oven for 10 min, as shown in Figure 4, sol–gel reactions of TEOS readily occurred and a sponge-like network structure emerged. When the reactions proceeded further to 20 and 30 min, void spaces in the spongy structure expanded while the ligaments that form the 3D networks became thinner, resembling wire-like features (Figure 4). The mSiO$_2$ nanowires were more apparent at 40 min, and they became fully developed after aging for 50 min (Figure 4). It is noted that the silica nanowires are interlinked with each other, inherited from the starting 3D networks. This morphological evolution suggests a dissolution and reorganization (of the gel mixture of silicate oligomeric species and trapped organic templating molecules) process upon the reaction time. Additionally, similar structural development was also observed by adjusting synthesis parameters (e.g., amounts of TEOS, CTACl, and EtOH, Experimental Section; Figures S4–S6). To identify key parameters, we further carried out a series of experiments. First, microemulsion was formed by adding TEOS into the solution with the presence of surfactant CTACl under stirring at room temperature, which is critical to generate sponge-like gel precursor for the growth of interlinked mesoporous silica nanowires. In a control experiment, TEOS was added to the solution without stirring, resulting in a TEOS film on the water surface. Afterward, sol–gel reactions at this interface produced interconnected mesoporous silica spheres with various sizes (Figure S7). It has been reported that the hydrolysis (and subsequent condensation) of TEOS at the interface of water and oil (organic) phase yielded a mixture of mesoporous silica spheres and fibers.[11] Second, it is noted that the organic alkaline triethanolamine (TEA) has been proposed to have a chelating effect for controlling product morphology.[4] To verify the actual role of TEA, simple inorganic bases such as ammonia and sodium hydroxide were used in replacement of TEA. As shown in Figure 5 and Figure S8, interlinked mSiO$_2$ nanowires could also be synthesized successfully with either ammonia or sodium hydroxide as an alkaline substitute, indicating that the chelating role of TEA is not crucial in our approach. However, when more base catalyst was used, a higher rate of TEOS hydrolysis was observed, and the surface of mSiO$_2$ nanowires became less smooth with smaller aspect ratios. If too much base was used in the synthesis, the uniformity of mSiO$_2$ products could be lost entirely (Figure S9). Therefore, the amount of alkaline used in the synthesis can also provide an additional means for fine tuning product morphology.

It has been widely recognized that, by adjusting their concentration, quaternary cationic surfactants (e.g., CTAB and CTACl) can exist as rod-shaped micelles in the solution, which are responsible for forming mesoporous silica channels with hexagonal packing.[18,46] In view of the morphological evolution results in Figure 4 and Figures S4–S6, the actual roles of CTACl used in our work are needed to be further explored, especially when random arrangement of mesopores and significant 3D branching of nanowires are observed. Generally speaking, there are two types of synthetic mechanisms responsible for formation of mesoporous silica materials,

dx.doi.org/10.1021/cs400996j | ACS Catal. 2014, 4, 566–576

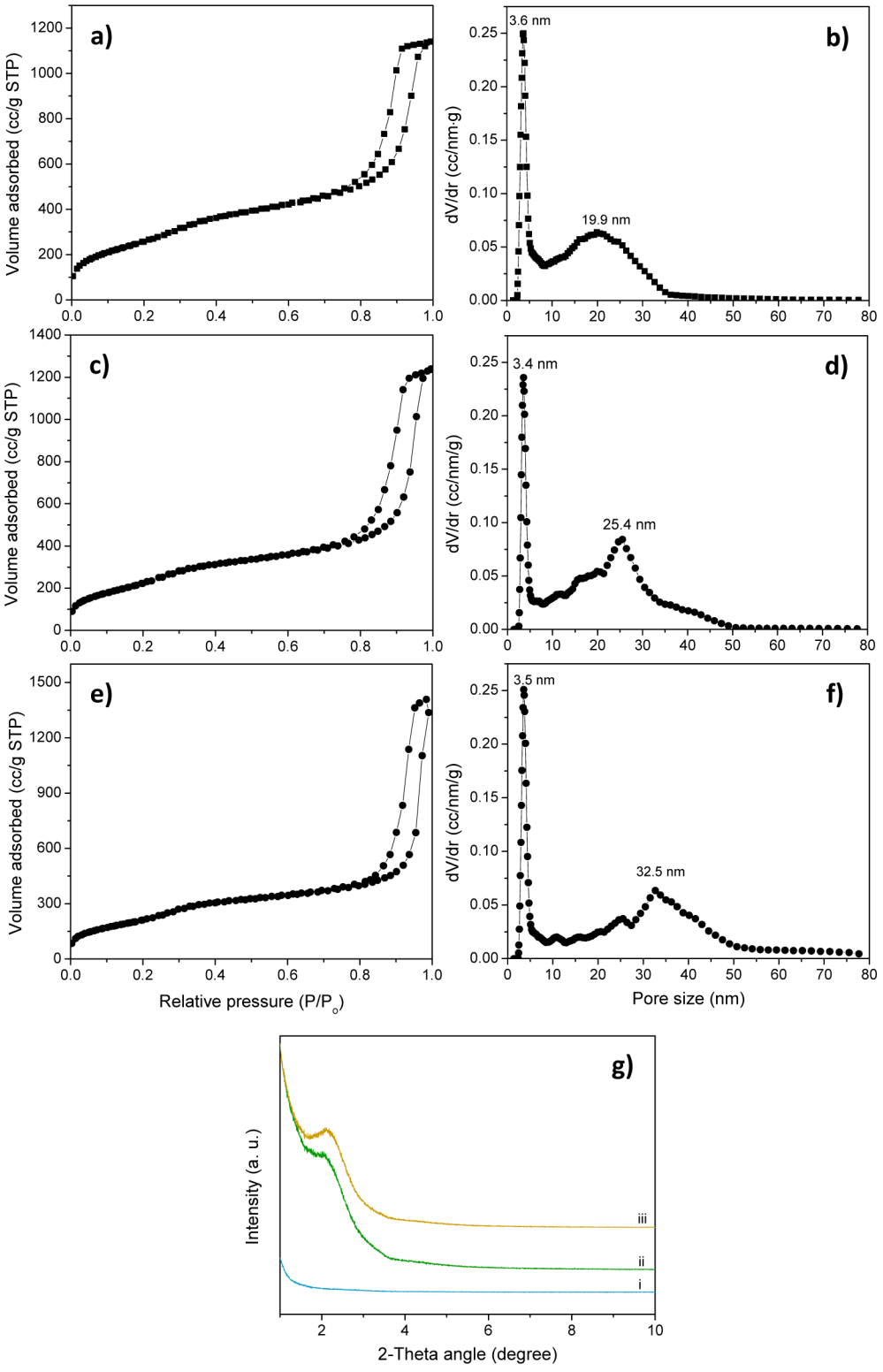

Figure 3. N_2 adsorption−desorption isotherms and pore size distributions of mesoporous silica nanowires synthesized with 0.5 mL (a,b), 1.0 mL (c,d), and 1.5 mL (e,f) of TEOS and small-angle XRD patterns (g) of mesoporous silica nanowires synthesized with 0.5 mL (i), 1.0 mL (ii), and 1.5 mL (iii) of TEOS.

cooperative self-assembly and the *liquid crystal templating process*.[1] Because our networked *m*SiO_2 nanowires were formed from the evolution of gel matrixes, the latter mechanism (i.e., "true" liquid crystal templating) can be ruled out unambiguously. To get more insight into the roles of CTACl playing, we further investigated the effects of this surfactant on final product morphology. By reducing the amount of CTACl to half or quarter of the initial value (Table S2), interlinked *m*SiO_2 spheres appeared instead of the *m*SiO_2 nanowires (Figure 6 and Figure S10). When too much CTACl (e.g., 4.0 mL) was used, however, very large mesoporous particles were also formed along with the normal *m*SiO_2 nanowires (Figure S11).

dx.doi.org/10.1021/cs400996j | *ACS Catal.* 2014, 4, 566−576

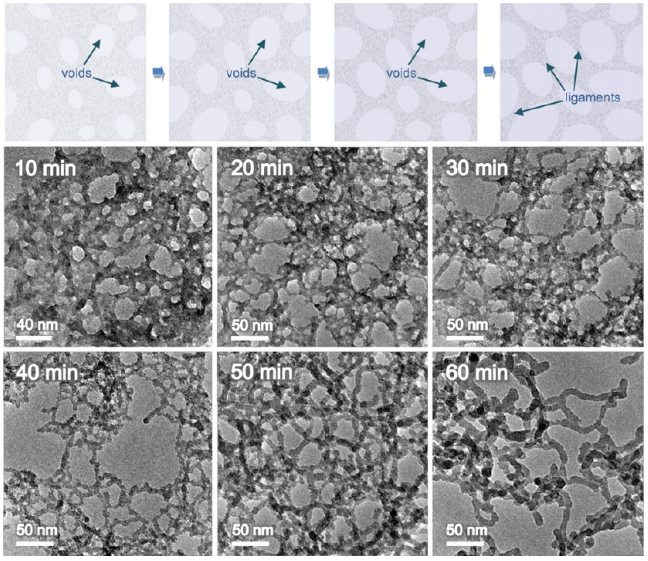

Figure 4. TEM images for evolution of silica gels (i.e., SiO_2 + CTACl) to interlinked mesoporous silica nanowires after different reaction times (10 to 60 min). Top panel illustrates the initial stage of void enlargement and development of interconnected ligaments (i.e., networked mesoporous silica nanowires) in the gel matrix.

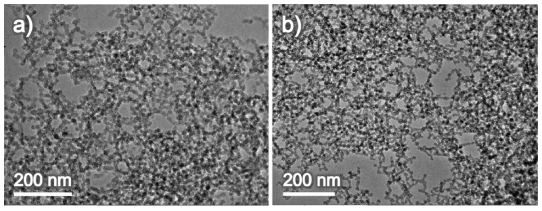

Figure 5. TEM images of interlinked mesoporous silica nanowires synthesized with (a) 0.1 mL of 1 M NH_4OH (pH ~10) and (b) 0.1 mL of 1 M NaOH (pH ~12) solution as alkaline sources.

In general, the (100) diffraction moved toward a lower 2θ angle when more CTACl was used, revealing an increasing trend in pore sizes (Figure 6c). It is thus recognized that an optimal amount of CTACl is also required to stabilize $m$$SiO_2$ nanowires, probably through establishing tubular micelles under our synthetic environments. In Figure 7, the effect of cosolvent was also examined by varying the amount of ethanol

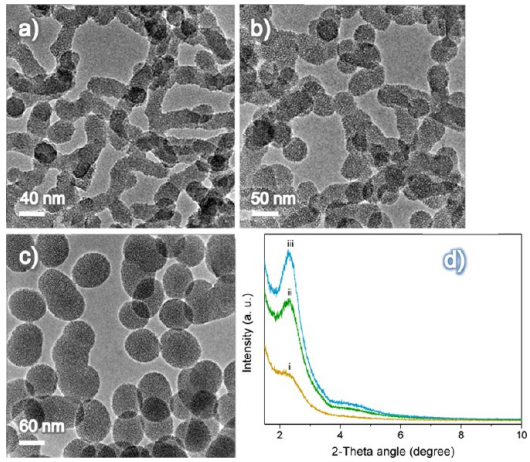

Figure 7. TEM images of interlinked mesoporous silica nanowires prepared with 2 mL (a), 3 mL (b), and 4 mL (c) of ethanol. Small-angle XRD patterns (d) of mesoporous silica nanowires synthesized with (i) 2 mL, (ii) 3 mL, and (iii) 4 mL of ethanol (Table S2).

from its normal value (1.0 mL, Experimental Section). When 2.0 mL of ethanol was used, the diameter of the $m$$SiO_2$ nanowires was increased to ~27 nm (Figure 7a, TEOS = 1.0 mL). When ethanol was further increased to 3.0 mL, the structure was composed of interlinked nanospheres with diameter of ~50 nm (Figure 7b). Using 4.0 mL of ethanol in synthesis, discrete mesoporous silica particles with diameters at ≈86 nm appeared (Figure 7c). A similar effect was observed with 0.5 mL of TEOS used in the synthesis (Figure S12). It has been reported that alcohols help elongate the cylindrical micelles formed by the quaternary ammonium surfactants for the formation of mesopores.[2] Indeed, in the present case, 1D channels were elongated and more parallel with more ethanol used, which is reflected in both wire/particle diameters (Figure 7a–c) and diffraction intensity of (100) peaks (Figure 7d). It is also believed that with more ethanol used, a more stable microemulsion of TEOS/ethanol (organic phase) in the water phase was formed, which acted as a template to grow mesoporous silica spherical particles together with the CTACl surfactant.

The influence of temperature on the formation of interlinked $m$$SiO_2$ nanowires was also studied (Figure S13). When the processing temperature was adjusted from 80 to 40 °C or even

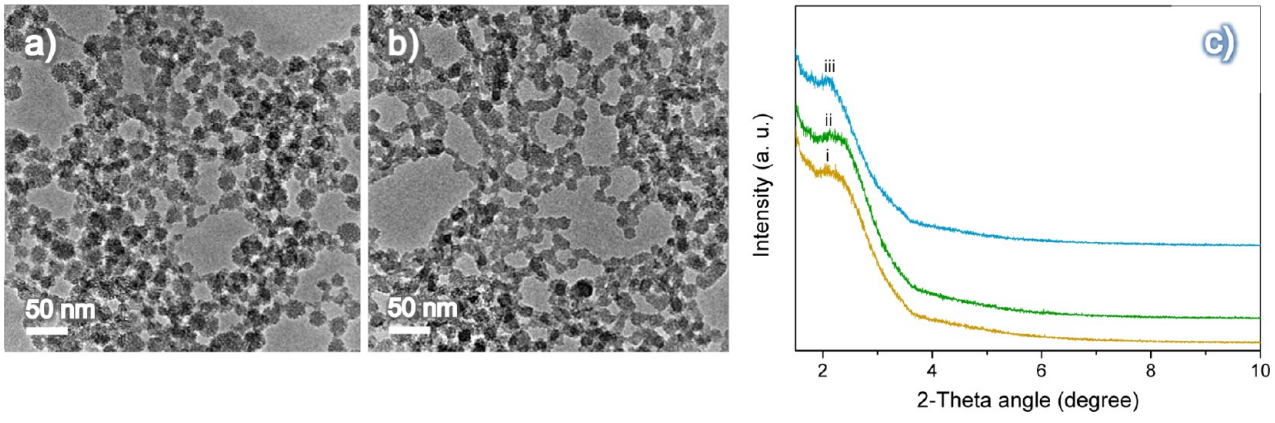

Figure 6. TEM images of interlinked mesoporous silica nanowires prepared with 0.5 mL (a) and 1.0 mL (b) of 25% CTACl solution. Small-angle XRD patterns (c) of interlinked mesoporous silica nanowires synthesized with (i) 0.5 mL, (ii) 1.0 mL, and (iii) 4.0 mL of 25% CTACl (see Table S2 and Figure S11).

dx.doi.org/10.1021/cs400996j | ACS Catal. 2014, 4, 566–576

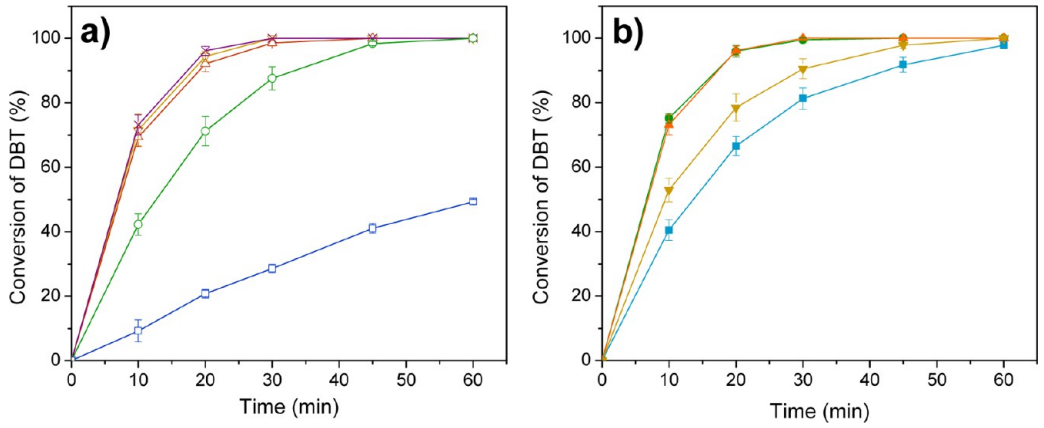

Figure 8. (a) Conversion of DBT with catalysts: 10% Mo-γ-Al_2O_3 (square), 10% Mo-fumed silica (circle), 10% Mo−1.0 mL of TEOS (triangle), 10% Mo−1.5 mL of TEOS (triangle, upside down), 10% Mo−0.5 mL of TEOS (cross). (b) Comparison of ODS activities of interlinked mesoporous silica nanowires with 2 (square), 5 (circle), 10 (triangle), and 15% (triangle, upside down) Mo loading. Reaction conditions: 10 mL of tetradecane (400 ppm S of DBT), 57 μL of TBHP, 50 mg of catalyst, 50 °C, 1200 rpm.

Table 1. Comparison of Oxidative Desulfurization of Model Diesel over Supported Molybdenum Catalysts[a]

entry	catalyst	S_{BET} (m^2/g)	Mo loading[b] (%)	conversion[c] (%)	TOF[d] (h^{-1})	sulfur concentration before reaction[e] (ppm)	sulfur concentration after reaction[f] (ppm)
1	2% Mo/*m*SiO_2 nanowires	852	2.6	81.3	22.3	400	94
2	5% Mo/*m*SiO_2 nanowires	699	5.2	99.5	20.7	400	16
3	10% Mo/*m*SiO_2 nanowires	560	7.8	100	13.4	400	13
4	10% Mo/*m*SiO_2 nanowires[g]	560	7.8	88.9	21.9	800	15
5	10% Mo/*m*SiO_2 nanowires[h]	560	7.8	72.7	30.1	1200	19
6	10% Mo/*m*SiO_2 nanowires[i]	560	7.8	98.0	13.5	400	201
7	10% Mo/*m*SiO_2 nanowires[j]	560	7.8	87.8	8.3	400	31
8	15% Mo/*m*SiO_2 nanowires	503	14.2	90.5	5.3	400	53
9	10% Mo/fumed silica	201	7.9	87.6	7.6	400	64
10	10% Mo/γ-Al_2O_3	89	6.8	28.5	1.9	400	303
11	10% Mo/SBA-15	488	8.9	96.9	11.0	400	18

[a]Reaction conditions: *n*-tetradecane (10 mL), dibenzothiophene (23 mg), *tert*-butyl hydroperoxide (57 μL), catalyst (50 mg), 50 °C. [b]Molybdenum loading was determined by EDX. [c]Conversion of dibenzothiophene at 30 min. [d]TOF was defined as mole of S converted per mole of Mo per hour at 10 min of reaction. [e]Sulfur concentration (ppm) before reaction was calculated as weight (in mg) of S atoms per liter of *n*-tetradecane solvent (1 ppm =1 mg of sulfur per liter of *n*-tetradecane). [f]Sulfur concentration (ppm) after reaction and adsorption at 30 min was determined from GC area of dibenzothiophene and dibenzothiophene sulfone. [g]Reaction conditions: *n*-tetradecane (10 mL), dibenzothiophene (46 mg), *tert*-butyl hydroperoxide (114 μL), catalyst (50 mg), 50 °C. [h]Reaction conditions: *n*-tetradecane (10 mL), dibenzothiophene (69 mg), *tert*-butyl hydroperoxide (171 μL), catalyst (50 mg), 50 °C. [i]Reaction conditions: *n*-tetradecane (5 mL), toluene (5 mL), dibenzothiophene (23 mg), *tert*-butyl hydroperoxide (57 μL), catalyst (50 mg), 50 °C. [j]Reaction conditions: *n*-tetradecane (10 mL), dibenzothiophene (23 mg), 30% H_2O_2 (31 μL), catalyst (50 mg), 50 °C.

to room temperature (~20 °C), there was no significant difference in the product morphology of *m*SiO_2 nanowires. However, when the temperature was increased to 100 °C, aggregative large particles were formed with regular nanowires in the final product, indicating that slow kinetics is favored for growth of silica nanowires. In addition, the reaction time was tested by prolonging the general reaction time of 2 h to 4−24 h (Figure S14). The morphology of silica nanowires remained unaltered after 6 h of the reaction (Figure S14b). However, irregularly shaped silica nanoparticles appeared after 8 h, and even more were formed after 24 h (Figure S14c−d). The above observation is additional evidence of dissolution and regrowth mechanism. Such a mechanism cannot be attributed to the *cooperative self-assembly* process either, although it likely bares certain cooperative features in the regrowth stage. On the basis of the above analysis, a formation mechanism could be proposed herein to account for the growth of networked *m*SiO_2 nanowires. Catalyzed in the alkaline solution, hydrolysis and condensation of TEOS in the mixed solvent of water/ethanol generated a spongy gel structure that serves both as a soft solid precursor and as an intrinsic scaffold to evolve into mesoporous nanowires through dissolution and regrowth processes (Figure 4). In addition its role of templating mesopores through formation of rod-shaped micelles, the surfactant CTACl is also believed to assemble into tubular micelles to stabilize branching 1D silica nanowires. Related to

dx.doi.org/10.1021/cs400996j | ACS Catal. 2014, 4, 566−576

this novel mechanism, control of growth rate by adjusting the concentrations of surfactant, alkaline, and cosolvent is critical to generate branching and thus final interlinked silica nanowire networks.

Catalyst−Adsorbent for Oxidative Desulfurization. The above networked mSiO$_2$ nanowires were used as catalyst support for molybdenum oxide for oxidative desulfurization (ODS) with model diesel. Silica nanowires with different aspect ratios were impregnated with 10 wt % Mo, and their activities were compared with commercial fumed silica and aluminum oxide supported with the same amount of metal loading (10 wt % Mo). As shown in Figure 8a, the conversion activities were quite similar for all mSiO$_2$ nanowires with different aspect ratios, that is, over 99% conversion of dibenzothiophene (DBT, $C_{12}H_8S$) was achieved at 30 min. The commercial fumed silica supported molybdenum catalyst was less active at an 87% conversion of DBT within the same reaction period, and the aluminum oxide supported catalyst is the least active with a 28% conversion of DBT at 30 min (Figure 8a and Table 1). Apparently, silica is a better support for molybdenum oxide used for ODS reaction compared to alumina, possibly because of a stronger acidity of silica (Figure 9 versus Figure S15; the

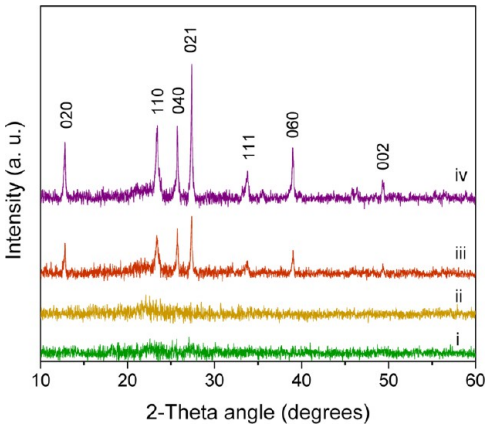

Figure 9. XRD patterns of interlinked mesoporous silica nanowires supported catalyst with: (i) 2%, (ii) 5%, (iii) 10%, and (iv) 15% Mo loading.

isoelectric point of SiO$_2$ is 1.7 to 3.5, and the isoelectric point of γ-Al$_2$O$_3$ is 7.0 to 8.0). The higher activity observed in the mSiO$_2$ supported catalysts could be attributed to a higher surface area, which ensures good dispersion of MoO$_3$ throughout the support surface. Besides, because of the small diameters of nanowires, shallow wormhole mesopores and hierarchical pore structures are also beneficial for DBT molecules to access the catalyst surface (see Figure 3 and Figure S16). The molybdenum loading effect was also studied by varying this aspect from 2 to 15% to optimize the DBT conversion. Shown in Figure 8b and Table 1, catalysts with 5 or 10% Mo loading exhibited the highest activities with 99.5 and 100% conversion, respectively, at 30 min, while 2 and 15% Mo/mSiO$_2$ nanowires were less active with 81.3 and 90.5% conversion at the same reaction time. However, when the activities (i.e., turn-over frequency (TOF), which is defined as a *mole of sulfur converted per mole of molybdenum per hour at 10 min of reaction*) of silica nanowires supported catalysts with 2−15% Mo loading were compared, 2% Mo/mSiO$_2$ nanowires were the most active catalysts with 22.3 h^{-1}. While the Mo loading increased to 5, 10 and 15%, the TOF value decreased to 20.7, 13.4, and 5.3 h^{-1} sequentially. In fact, the BET surface area of Mo/mSiO$_2$ nanowire catalysts dropped from 852 to 503 m^2/g when the Mo loading was increased from 2 to 15%. It is then understood that the dispersion of Mo is better at a lower loading, which accounts for the higher TOF values. The catalysts with 5 to 10% of Mo show the highest conversions of DBT (Figure 8b) because the interplay between total working catalyst and accessible surface area has been optimized. It should be mentioned that the performance (TOF) of our 10% Mo/mSiO$_2$ nanowire catalysts is even better than that of the 10% Mo/SBA-15 catalyst (Table 1) in which mean mesopores of silica phase are larger. Therefore, the excellent pore accessibility in our catalysts is once again proven.

The structural information of the Mo/mSiO$_2$ nanowire catalysts were examined by powder XRD, as displayed in Figure 9. For 2−5% Mo/mSiO$_2$ nanowires, no diffraction peaks are observed, indicating that molybdenum species were highly dispersed on the silica nanowires, while for 10 to 15% Mo/mSiO$_2$ nanowires, orthorhombic molybdenum trioxide α-MoO$_3$ phase (JCPDS card no. 05−0508, space group: *Pbnm*, a_o = 3.962 Å, b_o = 13.85 Å, and c_o = 3.697 Å) can be observed. The α-MoO$_3$ phase was also observed for the commercial fumed silica supported 10% Mo catalyst. It is noted that the α-MoO$_3$ peak intensity of 10% Mo/fumed silica (Figure S15) is much higher than that of the 10% Mo/mSiO$_2$ nanowires, revealing better metal dispersion on the silica nanowires support due to their large specific surface areas. For the 10% Mo/Al$_2$O$_3$ catalyst, three major peaks are found to be aluminum oxide phase (γ-Al$_2$O$_3$, JCPDS card no. 79−1558, space group: $Fd\bar{3}m$, a_o = 7.911 Å). Only two small peaks, (110) and (021), belong to the α-MoO$_3$ phase (Figure S15). It shows that molybdenum was also dispersed well on the Al$_2$O$_3$ support, though the activity is the lowest comparing to silica supported catalysts, which confirms that silica is a more active support than aluminum oxide for molybdenum oxide to be used for the ODS reaction. The morphology of the 10% Mo/mSiO$_2$ nanowire catalyst was examined by TEM/HRTEM/FESEM (Figure S16). It is noted that the mesoporous silica nanowire networks became more compact and integrated into much larger assemblages after calcination, while the molybdenum oxide (α-MoO$_3$) nanocrystals were distributed uniformly within the mesoporous silica. Consistent with the XRD results (Figure 9), the lattice spacing of 0.21 nm can be assigned to the (060) plane of α-MoO$_3$ phase. As 2−5% Mo/mSiO$_2$ catalysts are essentially amorphous, XPS analysis was carried out to study the oxidation state of supported molybdenum. Reported in Figure S17, the Mo $3d_{5/2}$ and Mo $3d_{3/2}$ peaks at 232.4 and 235.5 eV could also be assigned to Mo^{6+} oxidation state,[47] confirming the presence of well-dispersed Mo^{6+} oxide on the pore surfaces of mSiO$_2$ nanowires.

It is noted that the sulfur level of our model diesel was reduced drastically after the ODS reaction (Table 1). To understand this process, the model diesel was analyzed by GC-MS (Figures S18 and S19) before and after reaction. The GC peak of dibenzothiophene disappeared completely after the reaction, indicating that dibenzothiophene (DBT, $C_{12}H_8S$) had been oxidized to dibenzothiophene sulfone (DBTO, $C_{12}H_8O_2S$). Nevertheless, this product compound (e.g., DBTO) was not observable in the mass spectra (Figure S19), indicating DBTO adsorbed onto catalyst after reaction. When the used catalyst was washed by ethanol (or toluene), interestingly, dibenzothiophene sulfone could be found in the washing solvent (Figure S20). It thus reveals that the product

dx.doi.org/10.1021/cs400996j | ACS Catal. 2014, 4, 566−576

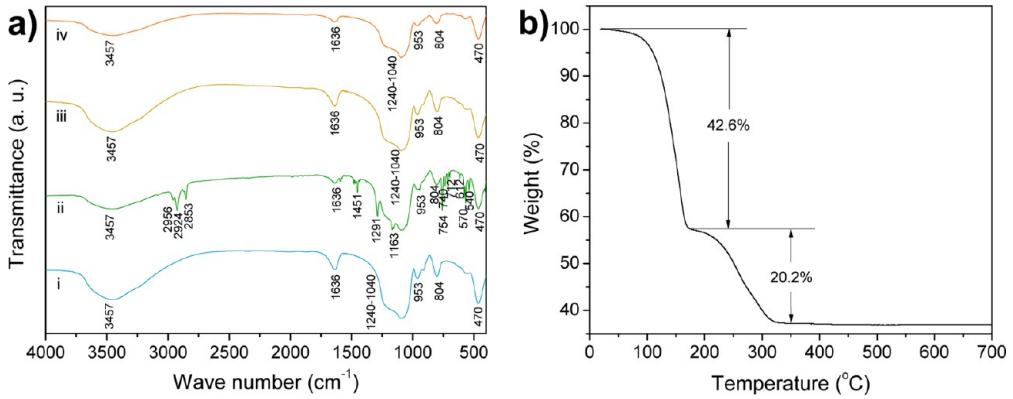

Figure 10. (a) FTIR spectra of (i) fresh 10% Mo/mSiO$_2$ nanowires, (ii) used 10% Mo/mSiO$_2$ nanowires, (iii) regenerated 10% Mo/mSiO$_2$ nanowires by calcination, and (iv) regenerated10% Mo/mSiO$_2$ nanowires by washing with toluene. (b) TGA of used 10% Mo/mSiO$_2$ nanowire catalyst.

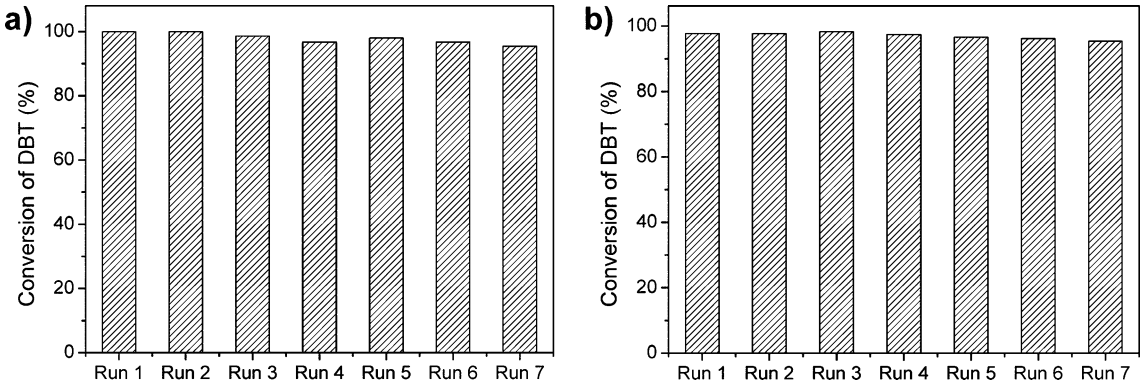

Figure 11. Recycle tests of 10% Mo/mSiO$_2$ nanowires regenerated by heating (a) and washing (b) with toluene.

dibenzothiophene sulfone was actually adsorbed on the catalyst after reaction, which explains why a very low concentration of sulfur was measured in the oxidized model diesel (Table 1). To further verify this observation, the fresh, used, and regenerated catalysts were characterized by Fourier-transformed infrared spectra analysis. For the fresh 10% Mo/mSiO$_2$ nanowire catalyst, the two peaks at 3457 and 1636 cm^{-1} correspond to adsorbed water or the surface −OH group, while the bands at 1240−1040, 804, and 470 cm^{-1} are attributed to asymmetric stretching, symmetric stretching, and bending modes of Si−O−Si bond of mesoporous silica nanowires, respectively (Figure 10a).[47] The peak at 953 cm^{-1} can be assigned to Mo═O of the supported molybdenum oxide. After the ODS reaction, more peaks other than those appeared in the fresh catalyst are observed in the FTIR spectra of used catalyst. The two peaks at 570 and 540 cm^{-1} correspond to wagging scissoring mode of −SO$_2$−, while those at 1291 and 1163 cm^{-1} are due to stretching mode of −SO$_2$− (of dibenzothiophene sulfone).[48] In addition, the peaks at 712, 754, and 740 cm^{-1} can be assigned to the C−S stretching mode, although the peaks at 754 and 740 cm^{-1} could also be due to wagging mode of four adjacent H within the aromatic ring as well.[48] The peaks at 612 and 1451 cm^{-1} are attributed to rocking and bending mode of C−H respectively, while the three peaks at 2853, 2924, and 2956 cm^{-1} are due to C−H stretching modes of adsorbed tetradecane.[48] On the basis of this FTIR analysis, it is confirmed that the product dibenzothiophene sulfone from our ODS process is adsorbed on the catalyst surface, reducing the sulfur content from an initial 400 ppm (as C$_{12}$H$_8$S) to less than 20 ppm (as C$_{12}$H$_8$S and/or C$_{12}$H$_8$O$_2$S) in the bulk solution phase of our model diesel. In addition to work as an ODS catalyst, rather intriguingly, the networked Mo/mSiO$_2$ nanowires can also function as an efficient adsorbent to remove their own reaction product (C$_{12}$H$_8$O$_2$S) from the diesel under the one-pot condition. Therefore, this consecutive conversion-cum-adsorption approach greatly simplifies conventional ODS processes where the sulfone products normally coexist with treated diesels/oils in the same liquid phase and requires further separation process to remove sulfone products by adsorption or extraction. In our present case, the used catalyst can be regenerated by thermal treatment at 300 to 500 °C to remove adsorbed dibenzothiophene sulfone (Figure 1b), as the FTIR spectrum of the regenerated catalyst is the same as that of the fresh one (no observable C−H or −SO$_2$− vibrations). To understand redox reactions involved in this regeneration process, furthermore, comparative XPS analysis was carried out for the catalysts. As shown in Figures S21 and S22, the oxidation state of Mo was +6 before the ODS reaction and was partially reduced to +5 after the reaction. After the regeneration, the +5 molybdenum oxide could be reoxidized back to +6 state (Figure S23). The used catalysts can also be regenerated through simple washing (Figure 1b). Interestingly, the toluene-washed catalyst (dried at 80 °C) showed +6 state for molybdenum as well, as the surface molybdenum could be easily oxidized in air with mild heating (Figure S24).[49] The S 2$p_{3/2}$ and S 2$p_{1/2}$ peaks located at 167.9 and 169.0 eV can be assigned to the S^{6+} of sulfone moiety in C$_{12}$H$_8$O$_2$S molecules.[50] The sulfur doublet disappeared after regeneration by

dx.doi.org/10.1021/cs400996j | ACS Catal. 2014, 4, 566−576

calcination or washing with toluene. The amount of adsorbed dibenzothiophene sulfone was further quantified by thermogravimetric analysis (Figure 10b). The weight loss at the first stage (20−172 °C) was due to evaporation of adsorbed water, while that at the second stage (172−325 °C) was attributed to the burnoff of the adsorbed ODS product. As a further confirmation for the latter assignment, the weight of adsorbed dibenzothiophene sulfone matches well with the amount of dibenzothiophene added in the reaction. The detailed calculation is illustrated in Supporting Information (Table S3).

The integrated system of Mo/mSiO$_2$ nanowire catalyst−adsorbent has been demonstrated to be very robust and stable through a series of recycling tests. The used Mo/mSiO$_2$ nanowires were recycled from the reaction mixture and calcined at 500 °C in air to remove adsorbed dibenzothiophene sulfone, before being used in the next experiment. Shown in Figure 11a, for example, the 10% Mo/mSiO$_2$ nanowire catalyst−adsorbent could maintain its good performance. At the seventh run, the conversion of DBT was still as high as 95.4% at 30 min of reaction, showing only a marginal change from the first run value (100%). In addition, the sulfur concentration in the liquid phase after the seventh run was determined to be only 33 ppm. In addition, the 10% Mo/mSiO$_2$ nanowire catalyst−adsorbent could also be regenerated by washing with toluene and recycled for 7 times without substantial loss of activity (Figure 11b). A further note should be taken is that the dimension of this catalyst−adsorbent is the regime of micrometers (Figure S16e,f, despite the wire diameter in nanoscale), which greatly eases the separation processes.

CONCLUSIONS

In summary, networked mesoporous silica nanowires have been synthesized by hydrolyzing TEOS under weak basic conditions. The thin silica nanowires (mean diameter ∼14 nm) which form a three-dimensional network structure have shallow wormhole channels aligning perpendicular to the nanowire axes. The aspect ratio of nanowire ligaments in the networks can be adjusted from 2:1 to 5:1 by reducing the amount of TEOS used in the synthesis. By calcination, the networks show hierarchical porosity originating from texture mesopores (3.6 nm) and framework mesopores (∼19.9 nm). The latter mesopores can also be tuned (e.g., from 19.9 to 32.5 nm) by reducing the concentration of TEOS in synthesis. The sponge-like gel structure formed at the initial stage has been identified as soft precursor/template for further dissolution and regrowth of the silica networks. In addition to its templating role to form the texture mesopores, the CTACl surfactant is also thought to stabilize resultant silica nanowires and thus to direct the growth of the overall networks. In addition, slow hydrolysis of TEOS is preferred for forming nanowires; the hydrolysis rate can be controlled by reaction temperature and/or concentration of alkaline. Taking advantage of their bimodal pore structure and large specific surface areas (e.g., 951 m^2/g), the silica nanowire networks were used to support molybdenum oxide catalyst for ODS reaction. The silica nanowire-based molybdenum oxide (α-MoO$_3$) catalyst is more active than commercial fumed silica and alumina-supported molybdenum catalysts. The high activity of our catalyst can be attributed to its tiered pore architecture for fast mass transport and large accessible working area. The optimal molybdenum loading was found to be 5 to 10% because of formation of highly dispersed molybdenum oxide nanoparticles in this range. Quite unexpectedly, the resultant dibenzothiophene sulfone was adsorbed on the catalyst surface. Therefore, the α-MoO$_3$−silica nanocomposite functions not only as an active catalyst but also as an effective adsorbent to remove the ODS product in a consecutive manner. Furthermore, the used α-MoO$_3$−silica catalyst−adsorbent system can be regenerated facilely by burning off the adsorbed sulfone or by solvent washing; the robustness of this bifunctional system has also been demonstrated.

ASSOCIATED CONTENT

Supporting Information

Experimental details and analysis data, TEM images, XRD patterns, and XPS spectra for materials characterization, and GC-MS spectra of ODS catalytic reactions. This material is available free of charge via the Internet at http://pubs.acs.org.

AUTHOR INFORMATION

Corresponding Author

*E-mail: chezhc@nus.edu.sg.

Notes

The authors declare no competing financial interest.

ACKNOWLEDGMENTS

The authors gratefully acknowledge the financial support provided by the National University of Singapore and GSK, Singapore.

REFERENCES

(1) Wan, Y.; Zhao, D. Y. *Chem. Rev.* **2007**, *107*, 2821−2860.
(2) Lin, H.-P.; Mou, C.-Y. *Acc. Chem. Res.* **2002**, *35*, 927−935.
(3) Niu, D. C.; Ma, Z.; Li, Y. S.; Shi, J. L. *J. Am. Chem. Soc.* **2010**, *132*, 15144−15147.
(4) Moller, K.; Kobler, J.; Bein, T. *Adv. Funct. Mater.* **2007**, *17*, 605−612.
(5) Yano, K.; Fukushima, Y. *J. Mater. Chem.* **2004**, *14*, 1579−1584.
(6) Bruinsma, P. J.; Kim, A. Y.; Liu, J.; Baskaran, S. *Chem. Mater.* **1997**, *9*, 2507−2512.
(7) Yang, Z. L.; Niu, Z. W.; Cao, X. Y.; Yang, Z. Z.; Lu, Y. F.; Hu, Z. B.; Han, C. C. *Angew. Chem., Int. Ed.* **2003**, *42*, 4201−4203.
(8) Tsung, C.-K.; Hong, W. B.; Shi, Q. H.; Kou, X. S.; Yeung, M. H.; Wang, J. F.; Stucky, G. D. *Adv. Funct. Mater.* **2006**, *16*, 2225−2230.
(9) Che, S. A.; Liu, Z.; Ohsuna, T.; Sakamoto, K.; Terasaki, O.; Tatsumi, T. *Nature* **2004**, *429*, 281−284.
(10) Wang, J. F.; Zhang, J. P.; Asoo, B. Y.; Stucky, G. D. *J. Am. Chem. Soc.* **2003**, *125*, 13966−13967.
(11) Huo, Q. S.; Zhao, D. Y.; Feng, J. L.; Weston, K.; Buratto, S. K.; Stucky, G. D.; Schacht, S.; Schuth, F. *Adv. Mater.* **1997**, *9*, 974−978.
(12) Sayari, A.; Han, B. H.; Yang, H. *J. Am. Chem. Soc.* **2004**, *126*, 14348−14349.
(13) Kosuge, K.; Sato, T.; Kikukawa, N.; Takemori, M. *Chem. Mater.* **2004**, *16*, 899−905.
(14) Zhao, D. Y.; Sun, J. Y.; Li, Q. Z.; Stucky, G. D. *Chem. Mater.* **2000**, *12*, 275−279.
(15) Wu, X. W.; Crudden, C. M. *Chem. Mater.* **2012**, *24*, 3839−3846.
(16) Mullner, M.; Lunkenbein, T.; Breu, J.; Caruso, F.; Muller, A. H. E. *Chem. Mater.* **2012**, *24*, 1802−1810.
(17) Ding, S. L.; Liu, N.; Li, X. W.; Peng, L. M.; Guo, X. F.; Ding, W. P. *Langmuir* **2010**, *26*, 4572−4575.
(18) Lin, H.-P.; Cheng, S. F.; Mou, C.-Y. *Chem. Mater.* **1998**, *10*, 581−589.
(19) Huesing, N.; Raab, C.; Torma, V.; Roig, A.; Peterlik, H. *Chem. Mater.* **2003**, *15*, 2690−2692.
(20) (a) Wang, D. P.; Zeng, H. C. *Chem. Mater.* **2011**, *23*, 4886−4899. (b) Yao, K. X.; Zeng, H. C. *Chem. Mater.* **2012**, *24*, 140−148.
(21) Zeng, H. C. *Acc. Chem. Res.* **2013**, *46*, 226−235.

(22) Chen, Y.; Chen, H. R.; Guo, L. M.; He, Q. J.; Chen, F.; Zhou, J.; Feng, J. W.; Shi, J. L. *ACS Nano* **2010**, *4*, 529−539.
(23) Qi, G. G.; Wang, Y. B.; Estevez, L.; Switzer, A. K.; Duan, X. N.; Yang, X. F.; Giannelis, E. P. *Chem. Mater.* **2010**, *22*, 2693−2695.
(24) Marlow, F.; McGehee, M. D.; Zhao, D. Y.; Chmelka, B. F.; Stucky, G. D. *Adv. Mater.* **1999**, *11*, 632−636.
(25) Wang, J. F.; Tsung, C.-K.; Hong, W. B.; Wu, Y. Y.; Tang, J.; Stucky, G. D. *Chem. Mater.* **2004**, *16*, 5169−5181.
(26) Kleitz, F.; Marlow, F.; Stucky, G. D.; Schuth, F. *Chem. Mater.* **2001**, *13*, 3587−3595.
(27) Li, N.; Wang, J.-G.; Zhou, H.-J.; Sun, P.-C.; Chen, T.-H. *Chem. Mater.* **2011**, *23*, 4241−4249.
(28) Kuang, D. B.; Brezesinski, T.; Smarsly, B. *J. Am. Chem. Soc.* **2004**, *126*, 10534−10535.
(29) Song, C. S.; Ma, X. L. *Appl. Catal., B* **2003**, *41*, 207−238.
(30) Qian, E. W. J. *Jpn. Petrol. Inst.* **2008**, *51*, 14−31.
(31) Lu, H. Y.; Gao, J. B.; Jiang, Z. X.; Jing, F.; Yang, Y. X.; Wang, G.; Li, C. *J. Catal.* **2006**, *239*, 369−375.
(32) Yazu, K.; Yamamoto, Y.; Furuya, T.; Miki, K.; Ukegawa, K. *Energy Fuels* **2001**, *15*, 1535−1536.
(33) Collins, F. M.; Lucy, A. R.; Sharp, C. *J. Mol. Catal. A: Chem.* **1997**, *117*, 397−403.
(34) Sampanthar, J. T.; Huang, X.; Dou, J.; Teo, Y. N.; Xu, R.; Wong, P. K. *Appl. Catal., B* **2006**, *63*, 85−93.
(35) Chang, J.; Wang, A. J.; Liu, J.; Li, X.; Hu, Y. K. *Catal. Today* **2010**, *149*, 122−126.
(36) Prasad, V. V. D. N; Jeong, K.-E.; Chae, H.-J.; Kim, C.-U.; Jeong, S.-Y. *Catal. Commun.* **2008**, *9*, 1966−1969.
(37) Garcia-Gutierrez, J. L.; Fuentes, G. A.; Hernandez-Teran, M. E.; Garcia, P.; Murrieta-Guevara, F.; Jimenez-Cruz, F. *Appl. Catal., A* **2008**, *334*, 366−373.
(38) Wang, D. H.; Qian, E. W.; Amano, H.; Okata, K.; Ishihara, A.; Kabe, T. *Appl. Catal., A* **2003**, *253*, 91−99.
(39) Ramirez-Verduzco, L. F.; Torres-Garcia, E.; Gomez-Quintana, R.; Gonzalez-Pena, V.; Murrieta-Guevara, F. *Catal. Today* **2004**, *98*, 289−294.
(40) Zhu, W. S.; Li, H. M.; Jiang, X.; Yan, Y. S.; Lu, J. D.; He, L. N.; Xia, J. X. *Green Chem.* **2008**, *10*, 641−646.
(41) Zhu, W. S.; Li, H. M.; Jiang, X.; Yan, Y. S.; Lu, J. D.; Xia, J. X. *Energy Fuels* **2007**, *21*, 2514−2516.
(42) Gao, G. H.; Cheng, S. F.; An, Y.; Si, X. J.; Fu, X. L.; Liu, Y. M.; Zhang, H. J.; Wu, P.; He, M. Y. *ChemCatChem* **2010**, *2*, 459−466.
(43) Chica, A.; Corma, A.; Domine, M. E. *J. Catal.* **2006**, *242*, 299−308.
(44) Hulea, V.; Fajula, F.; Bousquet, J. *J. Catal.* **2001**, *198*, 179−186.
(45) Ravikovitch, P. I.; Domhnaill, S. C. O.; Neimark, A. V.; Schuth, F.; Unger, K. K. *Langmuir* **1995**, *11*, 4765−4772.
(46) Chen, C. Y.; Xiao, S. Q.; Davis, M. E. *Microporous Mater.* **1995**, *4*, 1−20.
(47) Dou, J.; Zeng, H. C. *J. Am. Chem. Soc.* **2012**, *134*, 16235−16246.
(48) Patnaik, P. *Dean's Analytical Chemistry Handbook*; McGraw-Hill: New York, 2004.
(49) Dou, J.; Zeng, H. C. *J. Phys. Chem. C* **2012**, *116*, 7767−7775.
(50) Wei, X. M.; Zeng, H. C. *Chem. Mater.* **2003**, *15*, 433−442.